On the Strategy of Combining Coarse and Fine Grid Meshes in Numerical Weather Prediction

NORMAN A. PHILLIPS AND J. SHUKLA

Dept. of Meteorology, Massachusetts Institute of Technology, Cambridge 02139

(Manuscript received 3 April 1972, in revised form 13 April 1973)

ABSTRACT

A simple model containing gravity waves of phase speed C and a basic current U is used to test the hypothesis that in a nested grid system of different mesh sizes a better computation on the fine grid results if the outer, coarse-grid forecast is not made independently of the limited-area, fine-grid forecast but interacts with the fine grid throughout the integration. This hypothesis, which is based on an appeal to the characteristics of the differential equation, is verified by the tests, especially when C is less than U. A two-step Lax-Wendroff scheme with the staggered arrangement of variables suggested by Eliassen is used in both grids.

1. Introduction

The need to have a finer grid-point resolution in a limited area of a numerical forecast is a matter of considerable practical importance, since many of the most important weather-producing phenomena (hurricanes, squall lines) occur on a scale small enough that their adequate resolution requires a grid-point mesh which is too fine to be used over the entire forecast region (which may extend over the complete globe). On the other hand, these phenomena are not isolated from their surroundings and their evolution, therefore, cannot be computed independently of the flow patterns of larger scale in which they are imbedded.

There appear to be two basic strategies. In one, the complete large-scale prediction is first made on a coarse grid, completely independent of the fine-grid computation. Lateral boundary values for the fine-mesh forecast are then obtained as needed from a "history tape" of the coarse-mesh forecast (Hill, 1968; Wang and Halpern, 1970). We will refer to this as "one-way" interaction, or "strategy one." In the other strategy, the two forecasts are made simultaneously, i.e., the computation in the outer coarse mesh uses information predicted by the interior fine mesh. We will refer to this as "two-way" interaction or "strategy two." Birchfield (1960) followed this procedure in a non-divergent barotropic model and Koss (1971) and Ookochi (1972) have done so for a model based on the shallow-water equations. In the following section a brief argument is presented which favors the hypothesis that in a nested grid system of different mesh sizes a better computation on the fine grid results if the outer, coarse-grid forecast is not made independently of the limited-area, fine-grid forecast but interacts with the fine grid throughout the integration. This hypothesis is based on an appeal to the characteristics of the differential equation. In the remaining parts of the paper, the results of numerical integrations performed to test the aforesaid hypothesis are presented. This investigation was originally stimulated by receipt of a preprint of the paper by Harrison and Elsberry (1972) in which the second strategy is followed.

2. An argument based on an appeal to characteristics

Let us consider the simple problem of gravity waves on a uniform basic current U. (For simplicity we take $U \geqslant 0$.) To the extent we are permitted to linearize the meteorological equations, separate out the vertical dependence, and ignore the Coriolis force, heating and friction, the partial differential equations are

$$\left.\begin{aligned} \frac{\partial u}{\partial t} + U\frac{\partial u}{\partial x} &= -\frac{\partial \phi}{\partial x} \\ \frac{\partial \phi}{\partial t} + U\frac{\partial \phi}{\partial x} &= -C^2\frac{\partial u}{\partial x} \end{aligned}\right\}. \tag{1}$$

The speed C can assume a series of values, each associated with a different vertical wavenumber. Benwell and Bretherton (1968), for example, report values of 286, 111, 43.5, 26 and 16 m sec^{-1} for the five largest values of C for a particular 10-level hydrostatic baroclinic model. The largest value of C for a numerical hydrostatic model with many levels is expected to approach the "Lamb wave" speed, which is known from observations and theory to be about 320 m sec^{-1}. Smaller values of C are approximately equal to $NL_z/$

(2π), when N is the buoyancy frequency and L_z the vertical wavelength. The situation most commonly considered by meteorologists, however, is only that in which $C>U$ (e.g., Charney, 1962, p. 133). This occurs in barotropic versions of the hydrostatic system of equations when the mean value $\bar{\phi}$ of the geopotential is chosen to correspond to that at the 500-mb level: $C^2=\bar{\phi}\approx g\times 6$ km$\approx$ (246 m sec^{-1})^2.

The general solution of Eqs. (1) is

$$\left.\begin{aligned} u&=\frac{1}{C}[f(\xi)+g(\eta)]\\ \phi&=f(\xi)-g(\eta)\end{aligned}\right\}, \tag{2}$$

in which the characteristic coordinates ξ and η are given by

$$\xi=x-(U+C)t,$$
$$\eta=x-(U-C)t.$$

In other words, the combination $Cu+\phi$ is a function only of $x-(U+C)t$ and is constant along any line of slope

$$\left(\frac{dx}{dt}\right)_{\xi}=U+C \tag{3}$$

in the x,t plane. The combination of $Cu-\phi$ is a function only of $x-(U-C)t$ and is therefore constant along any line of slope

$$\left(\frac{dx}{dt}\right)_{\eta}=U-C. \tag{4}$$

When $U>C$ both sets of characteristics have a positive slope, while $U<C$ results in oppositely signed slopes.

Suppose we consider now a region $0<x<L$ in the x,t plane as corresponding to a fine-mesh region imbedded in a surrounding region in which a coarse mesh is used for prediction. The true continuous solution in $0<x<L$ must satisfy (2). In the case $C>U$, we see that at the inflow point $x=0$, the combination $Cu-\phi$ is determined by previous conditions in $0<x<L$ while at the outflow point $x=L$ the combination $Cu+\phi$ is determined by previous conditions in $0<x<L$. At both boundaries one additional independent piece of information is needed beyond that supplied by $0<x<L$. The situation $C<U$ is different, however. In this case both characteristics have positive slope, leading to the conclusion that at the outflow point $x=L$ the solution for *both* u and ϕ is completely determined by antecedent conditions in $0<x<L$, whereas at the inflow point $x=0$ *both* u and ϕ are completely determined by antecedent conditions in the upstream region $(x<0)$.

In actual practice, the method of obtaining boundary grid-point values of variables at $x=L$ for a fine grid located in $0<x<L$ from a surrounding coarse mesh is not likely to involve logical instructions which examine (for example) the sign of $U-C$, especially in a three-dimensional space grid. In particular, the same grid-point values of variables would be sought from the coarse grid in the cases $U>C$ as in $U<C$. Yet the characteristic argument given above for the continuous equations suggests that at $x=L$ all of the information obtained from the coarse mesh should really have come completely from the fine-mesh region itself if $U>C$. Similarly, at $x=0$, the characteristic argument suggests that only some of the information obtained from the coarse mesh should have come from the coarse mesh region $x<0$ when $U<C$. It appeared reasonable to us that the "two-way" interaction procedure of meshing, which allows the coarse-mesh values near the internal boundary to be influenced by the fine-mesh computations, might give a more faithful reproduction of the proper transmission of information into and out of the fine mesh than would the one-way interaction. The reasoning is only intuitive, but readily subject to testing.

3. Numerical tests

The following version of the shallow-water equations was used:

$$\left.\begin{aligned} \frac{du}{dt}&=fv-\frac{\partial\phi}{\partial x}\\ \frac{dv}{dt}&=-fu-\frac{\partial\phi}{\partial y}+Y\\ \frac{d\phi}{dt}&=-\phi\left(\frac{\partial u}{\partial x}+\frac{\partial v}{\partial y}\right)\end{aligned}\right\}, \tag{5}$$

where f is a constant Coriolis parameter, and Y represents a fictitious constant applied force which serves to geostrophically balance a steady mean current U:

$$Y=fU, \tag{6}$$

without requiring a mean northward gradient of ϕ. In this way ϕ, u and v can all be treated as periodic in both x and y, thereby avoiding special lateral boundary conditions which might introduce irregularities into the numerical results and confuse the meshing aspect of the tests.

The equations were solved with a two-step, Lax-Wendroff scheme (see Appendix) based on the time- and space-staggered lattice suggested by Eliassen (1956; see also Phillips, 1960). This scheme is well-behaved computationally and does not require additional "smoothing" or periodic adjustments to avoid computational instability and "grid separation." The outer (coarse) mesh covered a 1200 km$\times$1200 km square region in which grid-point values were located 50 km apart. The inner (fine) mesh was located in the center of this area and covered a 600 km$\times$600 km

region in which grid-point values were located 25 km apart (Fig. 1). Cyclic boundary conditions were applied at the outer edges of the coarse mesh. Integration on the coarse mesh for one complete time step of 9 min is accompanied by calculation on the fine mesh for two complete time steps of 4.5 min each. At the end of each 9-min cycle, values at or near the common boundaries of the two meshes were interpolated as needed from the other mesh. This interpolation was performed by fitting the polynomial $a+bx+cy+dyx$ to four surrounding points, or in some cases, the polynomial $a+bx$ or $a+cy$ to two neighboring points in the staggered array.

Six sets of initial data were used. In each set, three 12-hr calculations were made, consisting of: (0) a control forecast on which a single fine mesh covered the entire 1200 km×1200 km region; (I) a one-way interaction in which the coarse grid covered the entire area, and its forecast was made independently of the fine grid but provided interpolated values every 9 min for the two outermost rows and columns of the fine grid; and (II) a "two-way" interaction in which computations on the central part of the coarse grid were omitted, with interior boundary values being obtained by interpolation from the fine mesh every 9 min and outer boundary values for the fine mesh again being interpolated at those times from the coarse mesh as in (I). The overlap between the two meshes for the two-way interaction is illustrated in Fig. 2. This overlap was designed to be as small as possible without requiring interpolation between values which had themselves been interpolated. This approach is similar to one of the computationally stable schemes tested by Ciment (1972) for the linear advection equation.

The initial data were defined by using simple x- and t-dependent linear perturbation solutions of (5) on the basic state $u=U$, $v=0$, $\phi=C^2=$constant. These are given by three waves with the phase $\psi=kx-\omega t$:

$$\text{Geostrophic wave:}\quad \left.\begin{aligned} &\omega=kU\\ &\phi=\hat{\phi}\cos\psi\\ &u'=0\\ &v'=-k\hat{\phi}f^{-1}\sin\psi \end{aligned}\right\}. \tag{7}$$

$$\text{Gravity waves:}\quad \left.\begin{aligned} &\omega=kU\pm(f^2+k^2C^2)^{\frac{1}{2}}\\ &\phi'=\hat{\phi}\cos\psi\\ &u'=\frac{(\omega-kU)}{kC^2}\hat{\phi}\cos\psi\\ &v'=\frac{f}{kC^2}\hat{\phi}\sin\psi \end{aligned}\right\}. \tag{8}$$

All of the data were based on $L=2\pi k^{-1}=600$ km, $C=20$ m sec^{-1}, $f=10^{-4}$ sec^{-1} and $\hat{\phi}=20$ m^2 sec^{-2}. The six sets of initial data were defined by using the above formulas with $t=0$ for the three waves, once with $U=10$ m sec^{-1} and once with $U=30$ m sec^{-1}:

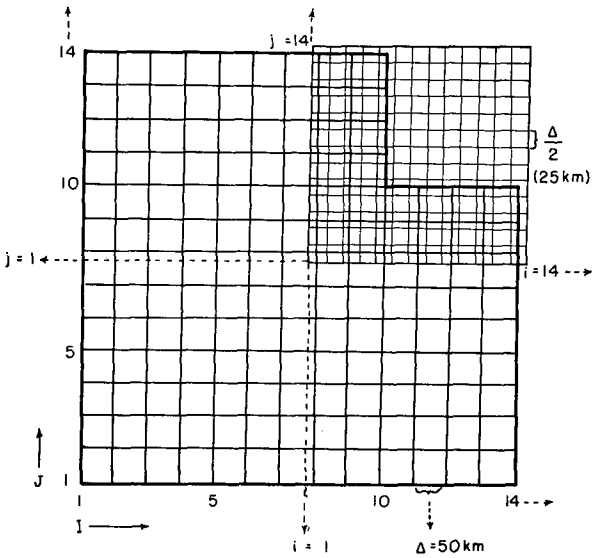

FIG. 1. Relative location of coarse and fine mesh over southwest quadrant of the whole area. (Due to symmetry, other quadrants are mere reflections of this.) The ϕ-field is physically located at the grid points defined by the intersection of perpendicular lines and other variables are located with respect to ϕ, in the way described in the Appendix. Capital and small letters refer to coarse- and fine-grid indices, respectively.

$$\left.\begin{aligned} u(t=0)&=U+u'(t=0)\\ v(t=0)&=0+v'(t=0)\\ \phi(t=0)&=C^2+\phi'(t=0) \end{aligned}\right\}. \tag{9}$$

The actual integration used the two-dimensional nonlinear equations (5), so the sinusoidal initial data became deformed with time, especially for some of the gravity wave cases. The two-dimensional meshed-grid structures also created some artificial y-dependence in the solution (the continuous solution theoretically remaining independent of y).

Integrations were performed only up to 12 hr because the purpose was not to examine the usefulness of meshing a fine and a coarse grid but simply to compare the two strategies.

Table 1 shows the root-mean-square errors at 12 hr over the entire 600 km×600 km fine mesh of the one-way (I) and two-way (II) forecasts, in which the control forecast (0) on a uniform fine mesh defined earlier is taken as the correct solution. (The errors for u and v are omitted in the geostrophic and gravity waves, respectively, because of their small amplitude.) The ϕ errors are largest in the positive gravity waves, where in 12 hr the wave has moved eastward about 1300 km for $U=10$ m sec^{-1} and 2200 km for $U=30$ m sec^{-1}, both distances being considerably farther than the 600 km width of the fine mesh. The important point for our present purpose however is that in all cases the error is smaller for two-way (II) than for the one-way (I) interaction. There is also a tendency for the im-

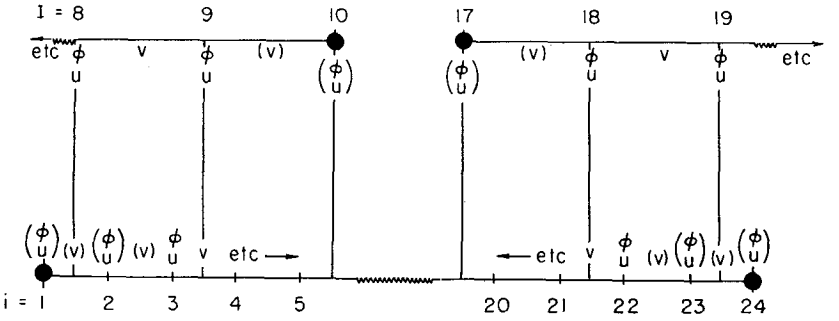

FIG. 2. Cross section along the x-axis through the fine-mesh region showing the relative position of variables on the coarse mesh (upper) and fine mesh (lower) at full time steps of the two-step Lax-Wendroff procedure. (In the staggered Eliassen arrangement, values of u are actually displaced northward $\Delta/2$ from the ϕ-points.) Indices I and i apply to the coarse and fine meshes. Heavy dots denote the extreme points of both grids in strategy II, and parentheses denote values obtained by interpolation from the other grid. In strategy I the coarse mesh extended completely across the central region with no values obtained on it by interpolation from the fine mesh.

provement in going from one-way to two-way interaction to be most marked when $U=30$ m sec^{-1}, greater than the 20 m sec^{-1} value for C. (The single exception to this is the ϕ error for the geostrophic wave.)

An indication of the spatial character of the error is given in Figs. 3–5, where a normalized expression for the variable part of the potential vorticity

$$\eta'=\frac{\bar{\phi}}{f}\left(\frac{f+\zeta}{\phi}-\frac{f}{\bar{\phi}}\right), \quad \zeta=\frac{\partial v}{\partial x}-\frac{\partial u}{\partial y},$$

is shown for the geostrophic wave case, and the divergence $(\partial u/\partial x)+(\partial v/\partial y)$ is shown for the two gravity wave cases. These were selected as more sensitive indicators than u,v and ϕ. The "correct" forecast is shown together with the results of strategy one and strategy two. In all figures the curves refer to the quantities at 12 hr along the x-axis passing through the center of the fine-mesh grid. (The region shown does not include the two extreme points at each end where values come from interpolations.) Although there are often appreciable differences between the control computation (0) and both (I) and (II), the (II) results are almost invariably nearer to (0) than those of (I), and are smoother.

The results of these numerical tests seem to indicate that for the integrations using nested grid systems, two-way interaction is more favorable than one-way interaction. One should, however, be careful about the stability of the finite-difference formulation of prediction equations (Ciment, 1972) so that the excitation of computational modes and nonlinear instabilities at the discontinuity in grid sizes may be reduced. The small-scale "wiggles" seem to appear near the boundary across which the correct wave pattern is leaving the fine mesh and moving into the coarse mesh. Values of the displacement speed of the patterns computed from grid-point values of ϕ show not only the expected improvement from an all coarse to an all fine mesh, but an improvement on the fine mesh in going from one-way to two-way interaction. For example, the geostrophic wave with $U=30$ m sec^{-1} gave values of

TABLE 1. Root-mean-square error (RMSE) for the six types of initial data, evaluated over the entire fine-mesh region. Positive and negative gravity waves correspond to the corresponding sign in the expression (8) for ω. The last three columns are the ratio in percent of the strategy II error to the strategy I error (see text for explanation).

Initial data: Disturbance wave	U (m sec^{-1})	Strategy	RMSE: u (m sec^{-1})	RMSE: v (m sec^{-1})	RMSE: ϕ (m^2 sec^{-2})	Percentage error ratio (II/I): u	v	ϕ
Geostrophic	10	I		0.292	1.809			
Geostrophic	10	II		0.278	1.472		95	81
Geostrophic	30	I		0.881	5.427			
Geostrophic	30	II		0.777	4.743		88	87
+Gravity	10	I	0.305		5.869			
+Gravity	10	II	0.293		5.697	96		97
+Gravity	30	I	0.370		7.199			
+Gravity	30	II	0.329		6.360	89		88
−Gravity	10	I	0.127		2.148			
−Gravity	10	II	0.124		2.097	98		98
−Gravity	30	I	0.099		1.913			
−Gravity	30	II	0.088		1.644	88		86

28.7, 28.8, 29.1 and 29.95 m sec^{-1} for displacement speeds on the all-coarse, one-way interaction, two-way interaction and all-fine grids, respectively.

The relative performance of the Lax-Wendroff scheme (L.W.) and a leap-frog (L.F.) finite-difference scheme was tested by integrating the one-dimensional version of Eqs. (5) using the six sets of initial data described in Section 3. In each set, four 48-hr calculations were made, consisting of: (i) a control forecast with L.W. in which a single fine mesh ($\Delta x=25$ km, $\Delta t=5$ min)

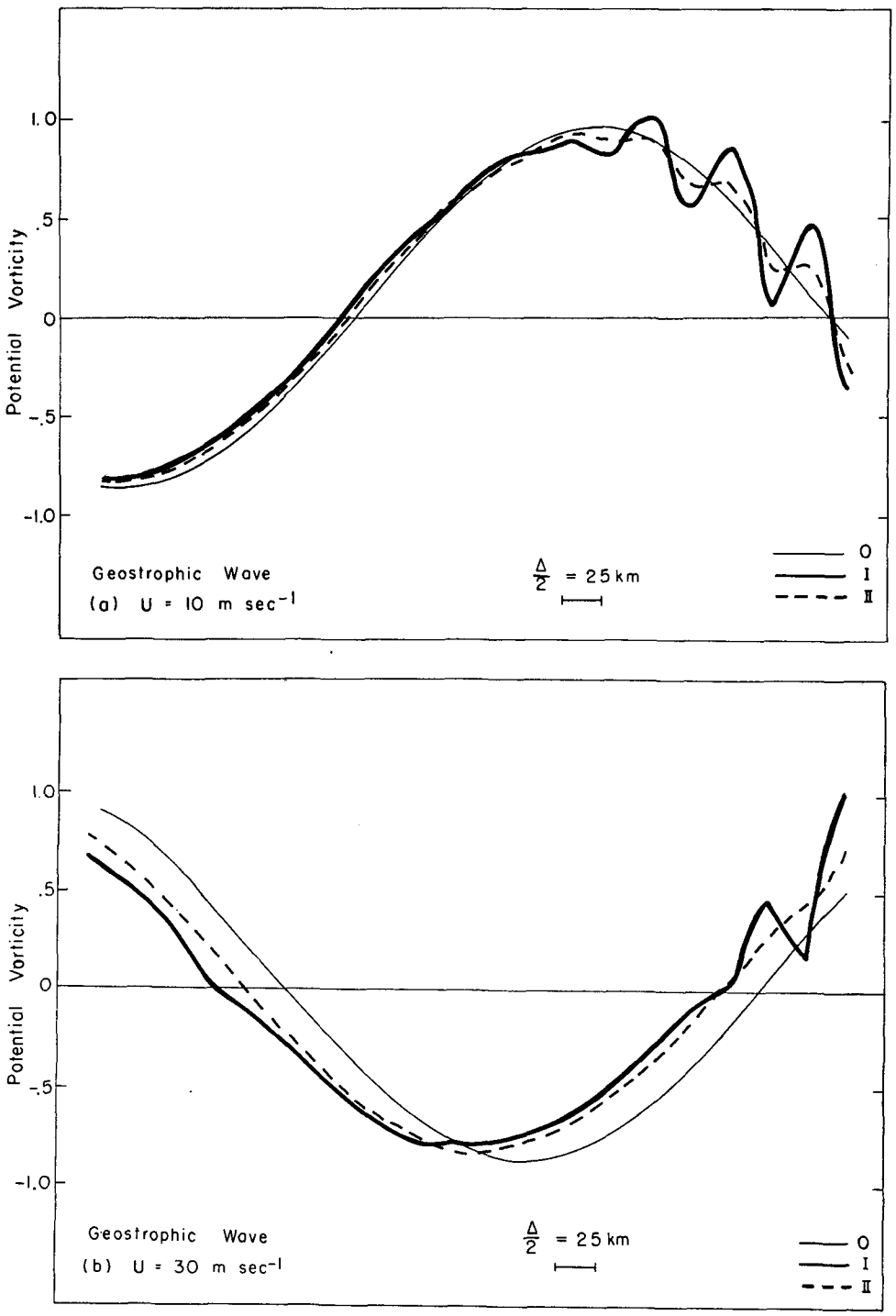

FIG. 3. Distribution of the variable part of the potential vorticity in the geostrophic wave case: (a) $U=10$ m sec^{-1}, (b) $U=30$ m sec^{-1}.

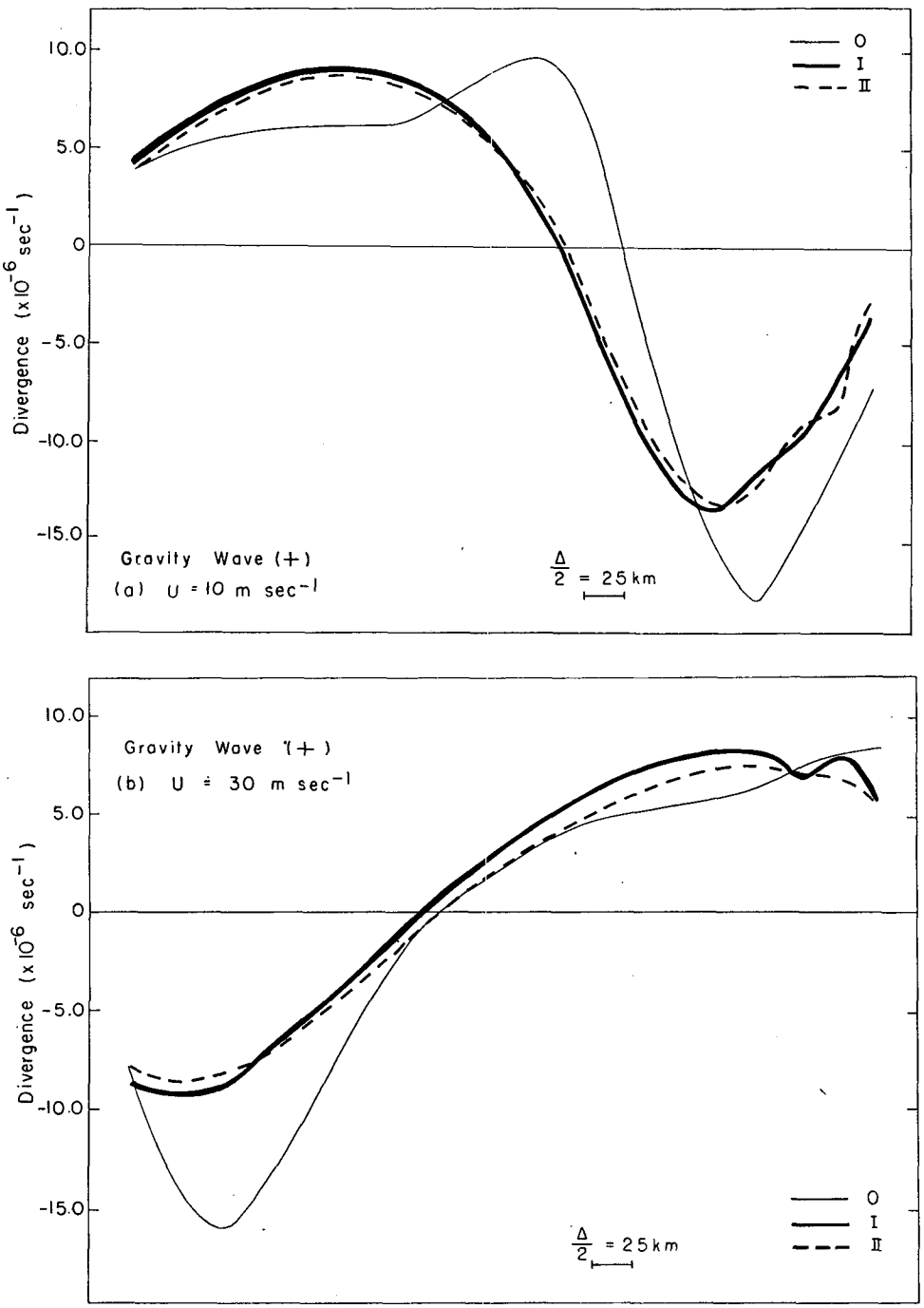

FIG. 4. Distribution of horizontal divergence (10^{-6} sec^{-1}) for the positive gravity wave: (a) $U=10$ m sec^{-1}, (b) $U=30$ m sec^{-1}.

covered the whole region, (ii) a "two-way" interaction forecast with L.W. in which $\Delta x=50$ km and $\Delta t=10$ min for the coarse mesh, (iii) a control forecast with L.F. in which a single fine mesh ($\Delta x=20$ km, $\Delta t=4.5$ min) covered the whole region, and (iv) a "two-way" interaction forecast with L.F. in which $\Delta x=40$ km, $\Delta t=9.0$ min for the coarse mesh. (Different values of Δx and Δt were chosen for the two schemes in order to equalize the computational arithmetic.) The L.W. calculations were done on a staggered grid (described in Section 3) and the L.F. calculations were done on a regular grid. Root-mean-square errors in the potential vorticity for the geostrophic wave and the divergence for the gravity waves were calculated over the fine

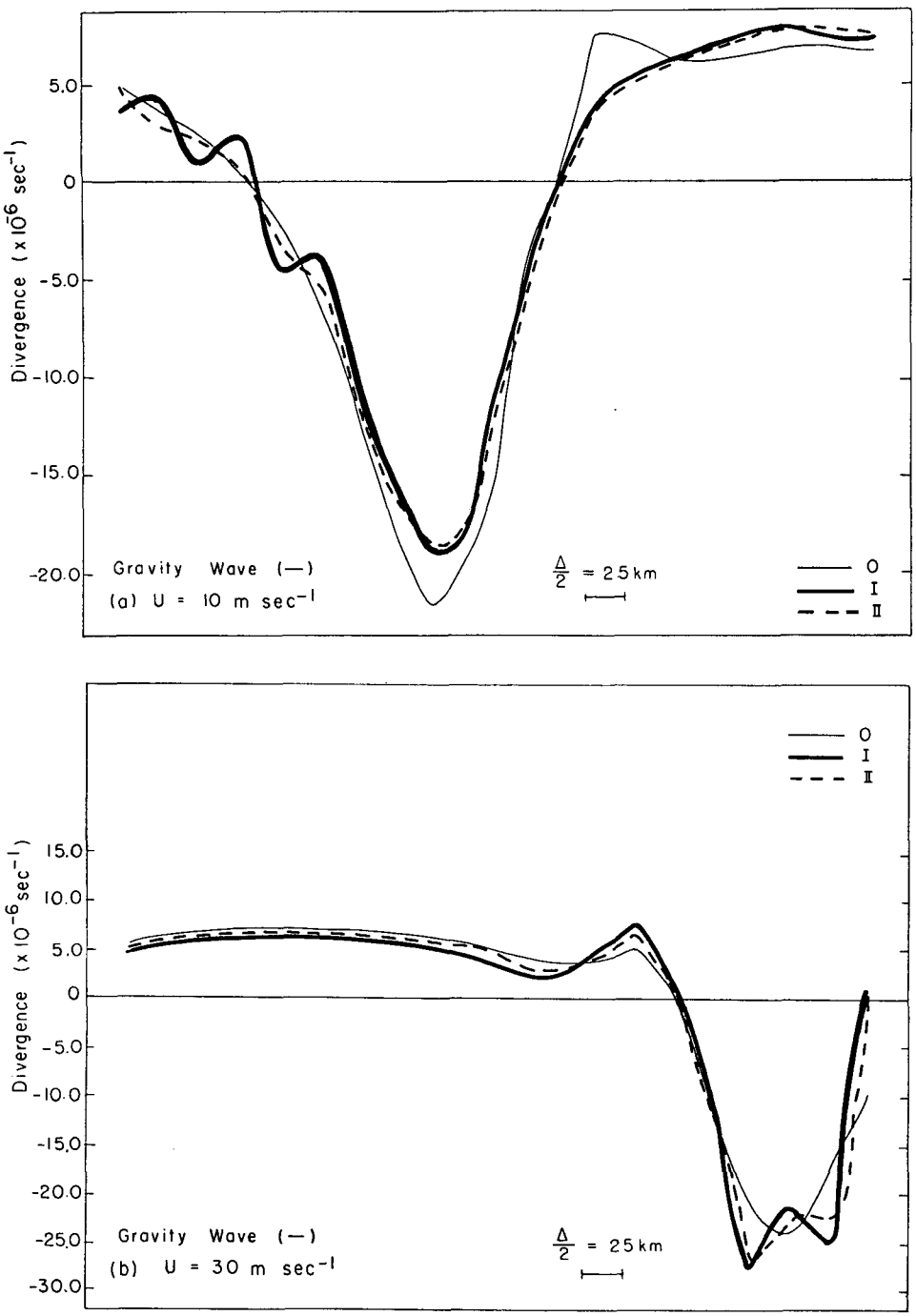

FIG. 5. Distribution of horizontal divergence (10^{-6} sec^{-1}) for the negative gravity wave: (a) $U=10$ m sec^{-1}, (b) $U=30$ m sec^{-1}.

mesh area between (i) and (ii) for L.W. and between (iii) and (iv) for L.F., respectively. It was found that for the 12-hr forecasts the errors defined in this way were generally more for the L.W. compared to the L.F. calculations, but for the 24-hr forecasts the errors for the L.F. calculations were more than for the L.W. calculations and this was even more true for the 48-hr forecasts.

Acknowledgments. This research was supported by the National Science Foundation under Grant A28724X with the Massachusetts Institute of Technology.

APPENDIX

Finite-Difference Equations

The time- and space-staggered lattice used here is the same as the one given earlier by Phillips (1960). The finite-difference expressions corresponding to the continuous equations (5) of the text are given below. The variables u_{ij} and v_{ij} are located $\Delta/2$ to the north and east of ϕ_{ij}, respectively, with the prime variables being valid at time $(n+\frac{1}{2})\Delta t$; ϕ'_{ij} is displaced $\Delta/2$ to the east and $\Delta/2$ to the north of ϕ_{ij}; and v'_{ij} and u'_{ij} are situated in the locations of u_{ij} and v_{ij}. [The primes here are different than in the initial data definitions of (9).] The following three full-time step equations

$$u_{ijn+1}-u_{ijn}$$
$$=-\sigma(\phi'_{ij}-\phi'_{i-1j})-\frac{\sigma}{4}[(u'_{ij}+u'_{i-1j})(u'_{ij}-u'_{i-1j})]$$
$$-\frac{\sigma}{4}[(u'_{ij+1}+u'_{i-1j+1})(u'_{ij+1}-u'_{i-1j+1})]+\lambda v'_{ij}$$
$$-\frac{\sigma}{2}v'_{ij}[u'_{ij+1}-u'_{ij}+u'_{i-1j+1}-u'_{i-1j}],$$

$$v_{ijn+1}-v_{ijn}$$
$$=-\sigma(\phi'_{ij}-\phi'_{ij-1})-\frac{\sigma}{4}[(v'_{ij}+v'_{ij-1})(v'_{ij}-v'_{ij-1})]$$
$$-\frac{\sigma}{4}[(v'_{i+1j}+v'_{i+1j-1})(v'_{i+1j}-v'_{i+1j-1})]-\lambda u'_{ij}$$
$$-\frac{\sigma}{2}u'_{ij}[v'_{i+1j}-v'_{ij}+v'_{i+1j-1}+v'_{ij-1}]+Y\Delta t,$$

$$\phi_{ijn+1}-\phi_{ijn}$$
$$=-\frac{\sigma}{2}[u'_{ij}(\phi'_{ij}+\phi'_{ij-1})-u'_{i-1j}(\phi'_{i-1j}+\phi'_{i-1j-1})]$$
$$-\frac{\sigma}{2}[v'_{ij}(\phi'_{ij}+\phi'_{i-1j})-v'_{ij-1}(\phi'_{ij-1}+\phi'_{i-1j-1})],$$

are computed using the half-time step variables u', v',ϕ' which have previously been computed from the equations

$$u'_{ij}=u^*_{ijn}-\frac{\sigma}{2}(\phi_{i+1j}-\phi_{ij})_n+\frac{\lambda}{2}v_{ijn},$$

$$v'_{ij}=v^*_{ijn}-\frac{\sigma}{2}(\phi_{ij+1}-\phi_{ij})-\frac{\lambda}{2}u_{ijn}+\frac{Y}{2}\Delta t,$$

$$\phi'_{ij}=\phi^*_{ijn}-\frac{\sigma}{8}[(\phi_{ij}+\phi_{i+1j}+\phi_{ij+1}+\phi_{i+1j+1})_n$$
$$\times(u_{i+1j}-u_{ij}+v_{ij+1}-v_{ij})_n].$$

In these equations $\sigma=\Delta t(\Delta)^{-1}$, $\lambda=f\Delta t$, where Δt and $\Delta=\Delta x=\Delta y$ are the time step and grid interval, respectively, such that $x=i\Delta x$, $y=j\Delta y$, $t=n\Delta t$. Asterisks denote the values of u, v, ϕ at $t=n\Delta t$ at the point upstream the distance $(-\bar{u}\Delta t/2, -\bar{v}\Delta t/2)$ from the point corresponding to the location of u',v',ϕ' at the half-time step. Overbars represent averages of the nearest surrounding values of u and v. Values of u^*, v^* or ϕ^* are obtained by interpolation with the polynomial $a+bx+cy+dxy$ fitted to the four surrounding points of u, v or ϕ, respectively.

REFERENCES

Benwell, G., and F. Bretherton, 1968: A pressure oscillation in a ten-level atmospheric model. *Quart. J. Roy. Meteor. Soc.*, **94**, 123–1313.

Birchfield, G. E., 1960: Numerical prediction of hurricane movement with the use of a fine grid. *J. Meteor.*, **17**, 406–414.

Charney, J., 1962: Integration of the primitive and balance equations. *Proc. Intern. Symp. Numerical Weather Prediction*, Tokyo, Meteor. Soc. Japan, 131–152.

Ciment, M., 1972: Stable difference schemes with uneven mesh spacings. *Math. Comput.*, **25**, 219–227.

Eliassen, A., 1956: A procedure for numerical integration of the primitive equations of the two-parameter model of the atmosphere. Sci. Rept. 4, Dept. Meteor., UCLA, 53 pp.

Harrison, E., and R. Elsberry, 1972: A method for incorporating nested finite grids in the solution of systems of geophysical equations. *J. Atmos. Sci.*, **29**, 1235–1245.

Hill, G., 1968: Grid telescoping in numerical weather prediction. *J. Appl. Meteor.*, **7**, 29–38.

Koss, W., 1971: Numerical integration experiments with variable resolution two-dimensional Cartesian grids using the box method. *Mon. Wea. Rev.*, **99**, 725–738.

Ookochi, Y., 1972: A computational scheme for the nesting of a fine mesh in the primitive equation model. *J. Meteor. Soc. Japan*, **50**, 37–48.

Phillips, N. A., 1960: Numerical integration of the hydrostatic system of equations with a modified version of the Eliassen finite difference grid. *Proc. Intern. Symp. Numerical Weather Prediction*. Tokyo, Meteor. Soc. Japan, 109–120.

Wang, H.-H., and P. Halpern, 1970: Experiments with a regional fine-mesh prediction model. *J. Appl. Meteor.*, **9**, 545–553.